JOURNAL OF SOLID STATE CHEMISTRY 98, 82–89 (1992)

Metal–Metal Bonding and Mixed-Valent Tantalum in $La_2Ta_3S_2O_8$

THEODORE D. BRENNAN AND JAMES A. IBERS

Department of Chemistry, Northwestern University, Evanston, Illinois 60208-3113

Received August 21, 1991; in revised form October 25, 1991

The compounds $La_2Ta_3S_2O_8$ and $La_2Nb_3S_2O_8$ have been prepared and characterized. From single-crystal X-ray diffraction measurements, $La_2Ta_3S_2O_8$ crystallizes in space group D_{2h}^{12}-*Pnnm* of the orthorhombic system with four formula units in a cell of dimensions $a = 9.876(7)$, $b = 11.768(7)$, and $c = 7.658(5)$ Å ($T = 111$ K). The compound is isostructural to a series of oxyselenides $Ln_2Ta_3Se_2O_8$ (*Ln* = La, Ce, Pr, and Nd) previously reported. The three-dimensional structure is built up from layers of tricapped trigonal-prismatically coordinated La atoms alternating with layers of octahedrally coordinated Ta atoms. One Ta atom is in a distorted octahedral site surrounded by six O atoms and forms edge-sharing dimers with itself. The other Ta atom is in a distorted octahedral environment with two O and four S atoms in its coordination sphere and forms edge-sharing chains with bridging S atoms. The one-electron band structure of $La_2Ta_3S_2O_8$ was calculated from the tight-binding method with an extended Hückel-type Hamiltonian. The band structure calculations support the hypothesis of separate Ta(+4) and Ta(+5) sites in the $Ln_2Ta_3Q_2O_8$ (*Q* = S and Se) compounds and point to the driving force behind the Ta–Ta pairing that occurs along the octahedral chains. $La_2Nb_3S_2O_8$ has the same structure, as deduced from a comparison of X-ray powder patterns.

Introduction

In a previous paper we described the synthesis and structure of the series of compounds $Ln_2Ta_3Se_2O_8$ (*Ln* = La, Ce, Pr, and Nd) (*1*). The structure consists of layers of Ta octahedra separated by the lanthanide cations. There are two crystallographically independent Ta sites within the layers. The first Ta site is coordinated by six O atoms and forms edge-sharing octahedral dimers. This structural unit has been observed previously for Ta in $CaTa_2O_6$ (*2*) and for Nb in α-$PrNb_3O_9$ (*3*). The second Ta site is coordinated by four Se and two O atoms and forms edge-sharing octahedral chains. The resultant $^1_\infty[Ta_2Se_4O_4^{8-}]$ chain was a previously unreported structural feature; it shows a metal–metal pairing distortion as found in the niobium and tantalum tetrahalides. The three other known structures of oxychalcogenides that involve lanthanides and early transition metals also contain edge-sharing octahedral chains of the rutile type, but they do not show the metal–metal bonding observed in $Ln_2Ta_3Se_2O_8$. $La_5V_3O_7S_6$ (*4*) contains two crystallographically independent V sites with separated $^1_\infty[VO_2S_2^{3-/5-}]$ sulfur-bridged chains. $CeCrOS_2$ (*5*) has two Cr sites with corner sharing between staggered $^1_\infty[CrS_6^{3-}]$ and $^1_\infty[CrO_2S_2^{3-}]$ sulfur-bridged chains to form $^2_\infty[Cr_2O_2S_4^{6-}]$ layers. $LaCrOS_2$ (*6*) has one Cr site that forms a $^1_\infty[Cr_2O_2S_4^{6-}]$ double chain.

We hypothesized that the first Ta site in $Ln_2Ta_3Se_2O_8$ could be formally assigned a +5 oxidation state and the second a +4 oxidation state (*1*). In this paper we describe the synthesis of $La_2Nb_3S_2O_8$ and $La_2Ta_3S_2O_8$ and the structure of the latter.

0022-4596/92 $5.00

It is isostructural with the oxyselenide series of compounds described earlier. We also show that one-electron band structure calculations on these oxychalcogenides support the assignments of formal oxidation states and account for the Ta–Ta pairing in the $^1_\infty[Ta_2Se_4O_4^{8-}]$ chains. The calculations are compared with those for NbX_4 (X = Cl, I) (*7*). We also report conductivity as a function of temperature for the $La_2Ta_3Se_2O_8$ and $Nd_2Ta_3Se_2O_8$ members of the series.

Experimental

Synthesis. To prepare $La_2Ta_3S_2O_8$ 0.5 g in total of powdered La_2S_3 (Strem, 99.9%), Ta_2O_5 (Aldrich, 99.99%), and Ta (AESAR, 99.98%) in a 1 : 1 : 1 ratio was loaded into a quartz tube that was subsequently evacuated to 10^{-4} Torr, sealed, and heated at 1475 K for 4 days. Black powder and rectangular black prisms were produced. Analysis of two such prisms with the microprobe of an EDAX-equipped Hitachi S-570 scanning electron microscope revealed the presence of La, Ta, and S in roughly a 1 : 2 : 1 ratio. The lack of reliable standards prevented quantitative analysis. One of the small prisms from the reaction was selected for a single-crystal X-ray diffraction study.

$La_2Nb_3S_2O_8$ was prepared in a similar manner by heating a 1 : 1 ratio of La_2S_3 and Nb_2O_5 (99.7%, City Chemical Corp.) powders in an evacuated quartz tube at 1275 K for 4 days. Crystals of $La_2Nb_3S_2O_8$ could be grown from the resultant powder by reheating at 1475 K or by extended heating at 1125 K with KBr as a flux.

Structure determination. The unit cell parameters for $La_2Ta_3S_2O_8$ were determined from the least-squares refinement of 12 reflections in the range $30° \leq 2\theta$ ($MoK\alpha_1$) $\leq 33°$ that had been automatically centered on a Picker FACS-1 diffractometer at 111 K. An examination of intensity data revealed Laue symmetry *mmm* and systematic absences $0kl$, $k + l$ odd and $h0l$, $h + l$ odd, consistent with space groups *Pnn*2 and *Pnnm*. Additional crystallographic details are given in Table I. During data collection 6 standard reflections measured after every 100 reflections showed no significant variation in intensity. All calculations were done on a Stardent ST2500 computer with methods and programs standard for this laboratory (*8*). Conventional atomic scattering factors (*9*) were used and anomalous-dispersion corrections (*10*) were applied. The processed data were corrected for absorption effects. The hkl and $hk\bar{l}$ reflections were averaged to give a satisfactory merging R index of 0.069, in support of the centrosymmetric space group *Pnnm* in which $Pr_2Ta_3Se_2O_8$ also crystallizes. Subsequent refinement of $La_2Ta_3S_2O_8$ confirmed the choice of *Pnnm*. The initial positions for the heavy atoms La, Ta, and S were obtained by use of the direct methods program SHELXS-86 (*11*). The oxygen atoms were located in subsequent difference electron density maps. The structure was standardized (*12*) according to the rules of Parthé and Gelato (*13*). The final cycle of isotropic refinement on F_0^2 resulted in values of $R(F_0^2)$ of 0.061 and $R_w(F_0^2)$ of 0.084. The value of $R(F_0)$ for those reflections having $F_0^2 > 3\sigma(F_0^2)$ is 0.033. The final difference electron density map shows no features greater than 1.4% the height of a Ta atom. For this reason and because the crystal is highly absorbing, refinement was terminated at the isotropic stage. The final positional and thermal parameters are given in Table II. Structure amplitudes are given in Table III.[1]

[1] See NAPS document No. 04919 for 6 pages of supplementary materials. Order from ASIS/NAPS, Microfiche Publications, P.O. Box 3513, Grand Central Station, New York, NY 10163. Remit in advance $4.00 for microfiche copy or for photocopy, $7.75. All orders must be prepaid. Institutions and Organizations may order by purchase order. However, there is a billing and handling charge for this service of $15. Foreign orders add $4.50 for postage and handling, $1.75 postage for any microfiche orders.

TABLE I

CRYSTALLOGRAPHIC DETAILS FOR $La_2Ta_3S_2O_8$

Formula	$La_2Ta_3S_2O_8$
Molecular weight (amu)	1013
Space group	D_{2h}^{12}-*Pnnm*
a (Å)	9.876(7)
b (Å)	11.768(7)
c (Å)	7.658(5)
V (Å^3)	890
Z	4
T (K)	111[a]
Crystal volume (mm^3)	5.87×10^{-4}
Crystal shape	Truncated octahedron ≈ 0.10 × 0.09 × 0.10 mm bound by {010}, {110}, {011}
Radiation	Mo graphite monochromatized ($\lambda(K\alpha_1)$ = 0.7093 Å)
Linear absorption coefficient (cm^{-1})	464
Transmission factors	0.035–0.102[b]
Detector aperture (mm)	Horizontal, 5.5; vertical, 4.0, 32 cm from crystal
Scan type	2θ
Scan speed	2°/min in 2θ
Scan range	±0.8° in 2θ
2θ limits (°)	$3 \leq 2\theta(\text{Mo}K\alpha_1) \leq 56$
Background counts	10 sec at each end of scan with rescan option[c]
Data collected	$+h, +k, \pm l$
p factor	0.04
Number of variables	38
No. of data collected	2160
No. of unique data	1165
No. of unique data with $F_0^2 > 3\sigma(F_0^2)$	913
$R(F^2)$	0.061
$R_w(F^2)$	0.084
R (on *F*, $F_0^2 > 3\sigma(F_0^2)$)	0.033
Error in observance of unit weight (e^2)	1.03

[a] The low-temperature system is based on a design by J. C. Huffman (*22*).

[b] The analytical method as employed in the Northwestern absorption program AGNOST was used for the absorption correction (*23*).

[c] The diffractometer was operated under the Vanderbilt disk-oriented system (*24*).

X-ray diffraction powder patterns were recorded for $La_2Ta_3S_2O_8$ and $La_2Nb_3S_2O_8$ with Cu$K\alpha$ radiation on an Enraf–Nonius Model FR-552 Guinier camera at 298 K. Unit cell parameters were calculated by a least-squares procedure; silicon (NBS Reference Material 640a) was used as an internal standard. For $La_2Ta_3S_2O_8$ a = 9.879(2), b = 11.779(2), and c = 7.659(2) Å (34 indexed lines); for $La_2Nb_3S_2O_8$ a = 9.886(3), b = 11.777(3), and c = 7.672(3) Å (24 indexed lines).

Physical measurements. Of the six known compounds in the $Ln_2M_3Q_2O_8$ series, for only two, $La_2Ta_3Se_2O_8$ and $Nd_2Ta_3Se_2O_8$, were there crystals large enough for conductivity measurements. Two crystals of each were mounted with Ag paint on Al wires of an integrated circuit chip can. Two-probe dc conductivity measurements were carried out along the *c* axis of both compounds with the use of a Fluke 8050A digital multimeter. Absolute conductivities were in the 200 nS (S = 1/Ω) range. Because of the difficulty in measuring the dimensions of the crystals and because two-probe measurements are affected by contact resistance, the absolute values of the conductivities are only approximate; however, only their temperature dependence is important for the determination of the energy gaps. The temperature was measured with a LakeShore DT-470 silicon diode temperature sensor in close proximity to the crystal. The can with the crystal was

TABLE II

X-RAY POSITIONAL PARAMETERS AND *B* (Å^2) FOR $La_2Ta_3S_2O_8$

Atom	Wyckoff position	*x*	*y*	*z*	*B* (Å^2)
La(1)	4*g*	0.20632(9)	0.33585(7)	0	0.33(2)
La(2)	4*g*	0.72755(9)	0.15519(7)	0	0.31(2)
Ta(1)	8*h*	0.36377(4)	0.08062(3)	0.24976(5)	0.24(1)
Ta(2)	4*e*	0	0	0.28398(9)	0.34(1)
S(1)	4*g*	0.0200(4)	0.1338(3)	0	0.45(5)
S(2)	4*g*	0.5173(4)	0.3458(3)	0	0.44(5)
O(1)	8*h*	0.3028(8)	0.4747(6)	0.2342(10)	0.3(1)
O(2)	8*h*	0.0573(9)	0.3969(6)	0.2555(10)	0.5(1)
O(3)	8*h*	0.2882(9)	0.2216(7)	0.2519(11)	0.7(1)
O(4)	4*g*	0.3486(11)	0.0515(8)	0	0.2(2)
O(5)	4*g*	0.1345(15)	0.5547(9)	0	0.6(2)

TABLE IV

ATOMIC PARAMETERS[a,b]

Orbital	ζ_1 (c_1)	ζ_2 (c_2)	H_{ii} (eV)
La			
6*s*	2.14		−7.67
6*p*	2.08		−5.01
5*d*	3.78 (0.7765)	1.381 (0.4586)	−8.21
Ta			
6*s*	2.28		−10.10
6*p*	2.241		−6.86
5*d*	4.762 (0.6815)	1.938 (0.6815)	−12.10
S			
3*s*	2.122		−20.0
3*p*	1.827		−11.0
O			
2*s*	2.275		−32.3
2*p*	2.275		−14.8

[a] The *d* orbitals are given as a linear combination of two Slater-type functions, and each is followed in parentheses by the weighting coefficient.

[b] A modified Wolfsberg–Hemholz formula was used to calculate $\mathbf{H}_{ij}$ (*25*).

placed in a brass sample holder within a Dewar vessel. The sample was cooled from boil-off gas from a liquid He reservoir; it was heated by placing the sample holder inside a glass tube wrapped in heating tape that was inside a small Dewar vessel. Cooling and heating rates were maintained at 0.5 to 2 K/min. Measurements were made in the temperature range 216 to 338 K for $La_2Ta_3Se_2O_8$ and 252 to 323 K for $Nd_2Ta_3Se_2O_8$.

Electronic structure. The one-electron band structures of the $^1_\infty[Ta_2S_4O_4^{8-}]$ chains, the $^2_\infty[Ta_6S_4O_{16}^{12-}]$ layers, and the $^3_\infty[La_4Ta_6S_4O_{16}]$ full unit cell were calculated with the use of the tight-binding scheme (*14–16*) by the extended Hückel method (*17, 18*). The atomic parameters employed in the calculations are summarized in Table IV (*19*). For ease of comparison with related calculations on $NbCl_4$ (*7*) the calculations were done with the *a* and *c* directions reversed from the crystal structure so that the $^1_\infty[Ta_2S_4O_4^{8-}]$ chains (Scheme 1) were along the *x*-direction. A 36-k-point set was used in the irreducible part of the Brillouin zone to calculate the average properties for the $^2_\infty[Ta_6S_4O_{16}^{12-}]$ layer.

Results

The structure of $La_2Ta_3S_2O_8$ is closely related to that of $Pr_2Ta_3Se_2O_8$ described earlier (*1*). Bond distances and angles for $La_2Ta_3S_2O_8$ are given in Table V. A labeled view of the unit cell is provided in Fig. 1. Additional views of this structure type have been presented previously (*1*). The structure comprises layers of octahedrally coordinated Ta atoms separated in the *b* direction by La sites that are tricapped trigonal prismatic. Atom Ta(2) is in a distorted octahedral site with *trans* O(1), *cis* S(1), and *cis* S(2) atoms. The Ta(2)–O(1) distance is 1.976(8) Å and the Ta(2)–S distances are 2.462(3) and 2.692(3) Å. The Ta(2)–O(1) distance is the same as that in $Pr_2Ta_3Se_2O_8$, 1.978(9) Å. In the *c* direction these Ta(2) octahedra are edge shared through S atoms to form a rutile-like chain. There are alternating short–long Ta(2)–Ta(2) separations of 3.309(2) and 4.350(2) Å. While the Ta(2)–Se bonds in $Pr_2Ta_3Se_2O_8$ (*1*) are longer than the present Ta(2)–S bonds, the Ta(2)–Ta(2) distances are shorter (3.272(2) and 4.328(2) Å). This chain of Ta(2) octahedra, $^1_\infty[Ta_2S_4O_4^{8-}]$, is corner shared through atom O(1) to the Ta(1) sites. Atom Ta(1) sits in a distorted octahedral site surrounded by six O atoms; the Ta–O distances range from 1.820(8) to 2.299(8) Å. These Ta–O distances are comparable to those in $CaTa_2O_6$ (1.85(3)–2.11(2) Å) (*2*) and $Pr_2Ta_3Se_2O_8$

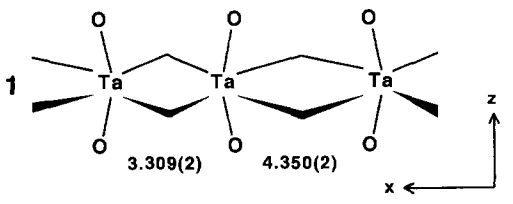

SCHEME I

TABLE V

DISTANCES (Å) AND ANGLES (°) IN $La_2Ta_3S_2O_8$

La(1)–O(3)	2×	2.486(8)	La(2)–O(4)		2.546(10)
La(1)–O(2)	2×	2.552(8)	La(2)–O(3)	2×	2.464(8)
La(1)–O(1)	2×	2.606(8)	La(2)–O(2)	2×	2.590(8)
La(1)–O(5)		2.671(11)	La(2)–O(1)	2×	2.652(8)
La(1)–S(1)		3.007(4)	La(2)–S(1)		2.899(5)
La(1)–S(2)		3.074(5)	La(2)–S(2)		3.056(4)
La(1)···Ta(1)		3.528(2)	La(2)···Ta(1)		3.489(2)
Ta(1)–O(3)		1.820(8)	Ta(2)–O(1)	2×	1.976(8)
Ta(1)–O(2)		1.930(9)	Ta(2)–S(2)	2×	2.462(3)
Ta(1)–O(5)		1.941(2)	Ta(2)–S(1)	2×	2.692(3)
Ta(1)–O(4)		1.949(2)	Ta(1)···Ta(1)		3.292(2)
Ta(1)–O(1)		2.067(8)	Ta(2)···Ta(2)		3.309(2)
Ta(1)–O(2)		2.299(8)	Ta(2)···Ta(2)		4.350(2)
O(3)–Ta(1)–O(2)		106.3(4)	O(1)–Ta(2)–O(1)		171.9(5)
O(3)–Ta(1)–O(5)		97.9(4)	O(1)–Ta(2)–S(2)		90.3(2)
O(3)–Ta(1)–O(4)		97.9(4)	O(1)–Ta(2)–S(2)		95.2(2)
O(3)–Ta(1)–O(1)		102.9(3)	O(1)–Ta(2)–S(1)		85.8(2)
O(3)–Ta(1)–O(2)		175.6(3)	O(1)–Ta(2)–S(1)		87.7(3)
O(2)–Ta(1)–O(5)		91.9(4)	S(2)–Ta(2)–S(2)		95.6(1)
O(2)–Ta(1)–O(4)		94.6(3)	S(2)–Ta(2)–S(1)		96.1(1)
O(2)–Ta(1)–O(1)		150.7(3)	S(2)–Ta(2)–S(1)		168.3(1)
O(2)–Ta(1)–O(2)		78.0(3)	S(1)–Ta(2)–S(1)		72.2(1)
O(5)–Ta(1)–O(4)		160.4(4)	Ta(2)–S(1)–Ta(2)		107.8(1)
O(5)–Ta(1)–O(1)		81.6(4)	Ta(2)–S(2)–Ta(2)		84.4(1)
O(5)–Ta(1)–O(2)		82.3(4)	Ta(1)–O(4)–Ta(1)		157.9(6)
O(4)–Ta(1)–O(1)		83.8(4)	Ta(1)–O(5)–Ta(1)		161.9(6)
O(4)–Ta(1)–O(2)		81.0(3)	Ta(1)–O(2)–Ta(1)		101.9(4)
O(1)–Ta(1)–O(2)		72.8(3)	Ta(2)–O(1)–Ta(1)		134.2(4)
O(3)–La(1)–O(3)		101.8(4)	O(4)–La(2)–O(3)		129.3(2)
O(3)–La(1)–O(2)		75.2(3)	O(4)–La(2)–O(2)		65.3(2)
O(3)–La(1)–O(2)		159.2(3)	O(4)–La(2)–O(1)		62.1(2)
O(3)–La(1)–O(1)		71.7(2)	O(4)–La(2)–S(1)		102.2(3)
O(3)–La(1)–O(1)		138.9(3)	O(4)–La(2)–S(2)		120.0(3)
O(3)–La(1)–O(5)		127.4(2)	O(3)–La(2)–O(3)		100.9(4)
O(3)–La(1)–S(1)		76.8(2)	O(3)–La(2)–O(2)		74.9(3)
O(3)–La(1)–S(2)		72.3(2)	O(3)–La(2)–O(2)		148.7(3)
O(2)–La(1)–O(2)		100.1(4)	O(3)–La(2)–O(1)		71.3(2)
O(2)–La(1)–O(1)		60.4(3)	O(3)–La(2)–O(1)		149.7(3)
O(2)–La(1)–O(1)		124.2(2)	O(3)–La(2)–S(1)		79.0(2)
O(2)–La(1)–O(5)		64.9(2)	O(3)–La(2)–S(2)		74.5(2)
O(2)–La(1)–S(1)		82.5(2)	O(2)–La(2)–O(2)		92.6(4)
O(2)–La(1)–S(2)		124.5(2)	O(2)–La(2)–O(1)		59.4(3)
O(1)–La(1)–O(1)		87.0(3)	O(2)–La(2)–O(1)		126.9(2)
O(1)–La(1)–O(5)		59.5(2)	O(2)–La(2)–S(1)		128.8(2)
O(1)–La(1)–S(1)		136.0(2)	O(2)–La(2)–S(2)		74.5(2)
O(1)–La(1)–S(2)		67.1(2)	O(1)–La(2)–O(1)		100.3(3)
O(5)–La(1)–S(1)		126.9(3)	O(1)–La(2)–S(1)		70.8(2)
O(5)–La(1)–S(2)		103.2(3)	O(1)–La(2)–S(2)		127.8(2)
S(1)–La(1)–S(2)		129.9(1)	S(1)–La(2)–S(2)		137.8(1)

(1.834(10)–2.325(9) Å) (*1*). The Ta(1)–O octahedra are edge shared through atom O(2) in the *a* direction and corner shared through atoms O(4) and O(5) in the *c* direction. These chains of corner-shared Ta–O octahedral dimers are also observed in $CaTa_2O_6$. The edge-shared Ta(1)–Ta(1) distance is 3.292(2) Å, compared to 3.327(2) Å in $Pr_2Ta_3Se_2O_8$ and 3.15 Å in $CaTa_2O_6$. Figure 2 compares polyhedral representations of the $CaTa_2O_6$ and $La_2Ta_3S_2O_8$ structures. The transformation from the $CaTa_2O_6$ to the $La_2Ta_3S_2O_8$ structure can be visualized as involving the separation of $[Ta_2O_{10}^{10-}]$ units in $CaTa_2O_6$ and addition of $^1_\infty[Ta_2S_4O_4^{8-}]$ chains to form $^2_\infty[Ta_6S_4O_{16}^{12-}]$ layers along with the substitution of La(+3) for Ca(+2).

In our earlier paper (*1*), we suggested the assignment of formal oxidation states in $Ln_2Ta_3Se_2O_8$ of $Ln(+3)$, Se(−2), and O(−2) to leave +14 charge units to be divided among three Ta atoms. We suggested that atom Ta(1), Wyckoff position 8*h*, coordinated by six O atoms, be taken as +5 and that atom Ta(2), Wyckoff position 4*e*, coordinated by two O and four S atoms, be taken as +4. This view was consistent with the presence of alternating short–long Ta(2)–Ta(2) distances that could arise from possible d^1–d^1 bonding interactions. Such interactions could lead to the small magnetic moment and poor conductivity observed in

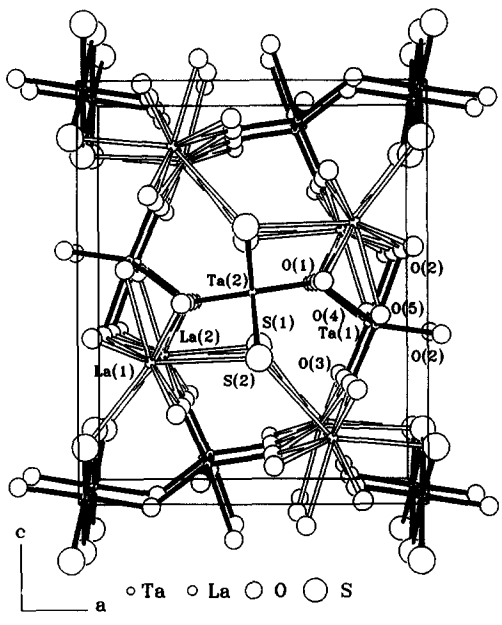

FIG. 1. A labeled view down the *c* axis of the $La_2Ta_3S_2O_8$ unit cell.

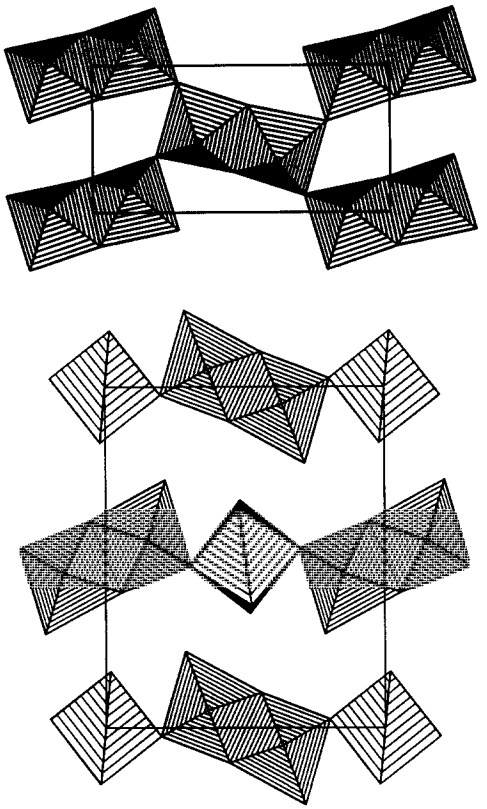

FIG. 2. A view showing the $[Ta_2O_{10}^{10-}]$ octahedral dimers in the $CaTa_2O_6$ (top) and $Ln_2Ta_3Q_2O_8$ (bottom) structures. Note that the Ta octahedral layers in $Ln_2Ta_3Q_2O_8$ comprise $[Ta_2O_{10}^{10-}]$ dimers and $^1_\infty[Ta_2S_4O_4^{8-}]$ chains.

$La_2Ta_3Se_2O_8$. Subsequently, we noted a similarity between the octahedral chains of the Ta(2) site and the chains in NbX_4 (*20*). Since a band-structure calculation was available for $NbCl_4$ (*7*), we carried out one for $La_2Ta_3S_2O_8$.

The t_{2g} *d*-block band structure of one Ta layer, $^2_\infty[Ta_6S_4O_{16}^{12-}]$, along the direction of the Ta(2) chains ($\Gamma \rightarrow \mathbf{X}$) and perpendicular to the chains ($\Gamma \rightarrow \mathbf{Z}$) is shown in Fig. 3. The bands that are composed mainly of Ta(2) *d*-orbitals are emphasized and labeled. Figure 3 shows the lowest *d*-bands that arise from the t_{2g}-symmetry Ta *d*-orbitals ($x^2 - y^2$, yz, and xy for Ta(2)). The band dispersion along the intralayer direction perpendicular to the Ta(2) chains ($\Gamma \rightarrow \mathbf{Z}$) is very small (less than 0.2 eV), an indication of highly localized Ta *d*-orbital interactions. Similarly, calculations on the complete unit cell show very little band dispersion along the interlayer direction ($\Gamma \rightarrow \mathbf{Y}$). The lowest lying Ta *d*-band is the bonding combination of the $d_{x^2-y^2}$ orbitals for Ta(2) (labeled $x^2 - y^2(+)$ in Fig. 3). The next highest band is the antibonding combination of the Ta(2) d_{yz} orbitals (labeled $yz(-)$ in Fig. 3). On the assumption of doubly occupied bands, the location of the Fermi level necessitates the *d*-block bands be filled up to the $x^2 - y^2(+)$ band for Ta(2). This implies that the Ta(2) atoms are formally +4 and the Ta(1) atoms are formally +5. The predicted band gap is ~0.42 eV. A plot of the density of states in the Ta t_{2g} *d*-block region is given in Fig. 4. Calculations that include La to give the band structure for the complete unit cell show the same features as those on only one Ta layer.

The electronic structure can be understood more simply by considering a single chain of distorted edge-sharing octahedra,

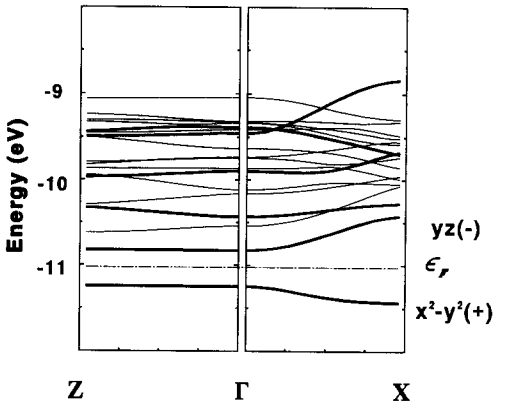

FIG. 3. *d*-Block t_{2g} band structure of the $^2_\infty[Ta_6S_4O_{16}^{12-}]$ layer as a function of wave vector **k** from $\Gamma \rightarrow \mathbf{Z}$ and $\Gamma \rightarrow \mathbf{X}$ with the $^1_\infty[Ta_2S_4O_4^{8-}]$ chain along the x direction. The bands emphasized with heavy lines have major orbital components that are combinations of the *d*-orbitals from atom Ta(2).

$^1_\infty[Ta_2S_4O_4^{8-}]$, formed by the +4 Ta(2) site. When the band structure of the complete Ta layer is compared to the band structure for the $^1_\infty[Ta_2S_4O_4^{8-}]$ chain, the bands attributed to Ta(2) are unchanged, justifying calculations on the separated chains. An idealized chain may be envisioned without the Ta(2) pairing distortion in which the $x^2 - y^2$ and yz bands are partially filled. When the idealized chain undergoes the pairing distortion, the $x^2 - y^2(+)$ band drops in energy and a band gap opens up. From calculations of the total energy, this idealized chain structure is unstable relative to the chains with Ta–Ta pairing. The results from calculations on the $^1_\infty[Ta_2S_4O_4^{8-}]$ chains parallel those for $NbCl_4$ (*7*) and are as expected for a doubly bridged MX_4 d^1 chain. The only significant differences between calculations on the $NbCl_4$ chains and on the $^1_\infty[Ta_2S_4O_4^{8-}]$ chains arise from the apical O atoms in the oxysulfide chain that distort the local octahedral symmetry.

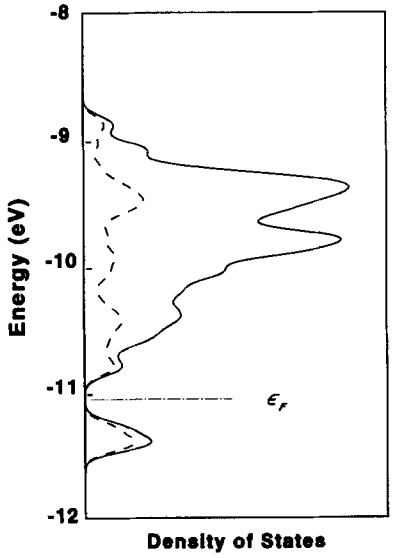

FIG. 4. Plot of the density of states in the Ta t_{2g} d-band region for a $^2_\infty[Ta_6S_4O_{16}^{12-}]$ layer. The solid line is the total density of states and the dashed line is the contribution from atom Ta(2).

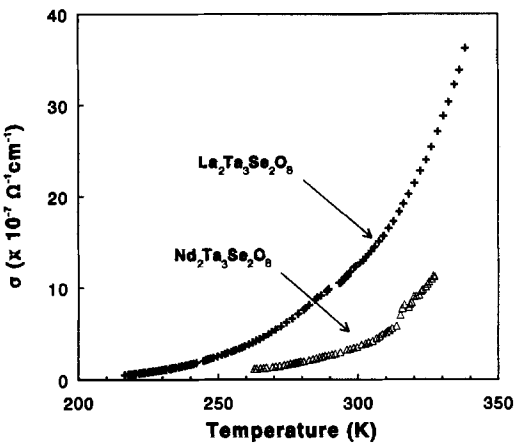

FIG. 5. The temperature-dependent electrical conductivity along the c direction of crystals of $La_2Ta_3Se_2O_8$ and $Nd_2Ta_3Se_2O_8$. The value of σ_{298K} is $\sim 1.2 \times 10^{-6}$ Ω^{-1} cm^{-1} for $La_2Ta_3Se_2O_8$.

Although conductivity measurements were not possible on $La_2Ta_3S_2O_8$, the conductivities of $La_2Ta_3Se_2O_8$ and $Nd_2Ta_3Se_2O_8$ decrease with decreasing temperature, indicating semiconducting behavior. For an intrinsic semiconductor, temperature dependence of the carrier concentration, and therefore conductivity, is dominated by the exponential term, $\exp(-E_g/2k_BT)$ (*21*). Plots of the conductivity along the c direction of $La_2Ta_3Se_2O_8$ and $Nd_2Ta_3Se_2O_8$ as a function of temperature are shown in Fig. 5. From these data band gaps of 0.43(2) and 0.54(6) eV are calculated for $La_2Ta_3Se_2O_8$ and $Nd_2Ta_3Se_2O_8$, respectively. These experimental energy gaps agree approximately with those expected from the band structure calculations on $La_2Ta_3S_2O_8$.

Acknowledgments

This research was supported by the U.S. National Science Foundation—Solid State Chemistry Grant DMR-88-13623. Use was made of the Scanning Electron Microscope Facility of Northwestern University's Material Research Center supported by NSF Grant DMR 88-21571. We thank Professor Jeremy Burdett and Mr. John Mitchell for helpful discussions concerning the band structure calculations.

References

1. T. D. Brennan, L. E. Aleandri, and J. A. Ibers, *J. Solid State Chem.* **91,** 312 (1991).
2. L. Jahnberg, *Acta Chem. Scand.* **17,** 2548 (1963).
3. C. C. Torardi, L. H. Brixner, and C. M. Foris, *J. Solid State Chem.* **58,** 204 (1985).
4. J. Dugue, T. Vovan, and P. Laruelle, *Acta Crystallogr. C* **41,** 1146 (1985).
5. J. Dugue, T. Vovan, J. Villers, *Acta Crystallogr. B* **36,** 1294 (1980).
6. J. Dugue, T. Vovan, and J. Villers, *Acta Crystallogr. B* **36,** 1291 (1980).
7. M.-H. Whangbo and M. J. Foshee, *Inorg. Chem.* **20,** 113 (1981).
8. J. M. Waters and J. A. Ibers, *Inorg. Chem.* **16,** 3273 (1977).
9. "International Tables for X-Ray Crystallography," Vol. IV, Tables 2.2A and 2.3.1, Kynoch Press, Birmingham (1974).
10. J. A. Ibers and W. C. Hamilton, *Acta Crystallogr.* **17,** 781 (1964).
11. G. M. Sheldrick, *in* "Crystallographic Computing 3" (G. M. Sheldrick, C. Kruger, and R. Goddard, Eds.), pp. 175–189, Oxford Univ. Press, London (1985).
12. L. M. Gelato and E. Parthé, *J. Appl. Crystallogr.* **20,** 139 (1987).
13. E. Parthé and L. M. Gelato, *Acta Crystallogr. A* **40,** 169 (1984).
14. M.-H. Whangbo and R. Hoffmann, *J. Am. Chem. Soc.* **100,** 6093 (1978).
15. M.-H. Whangbo, R. Hoffmann, and R. B. Woodward, *Proc. R. Soc. London Ser. A* **366,** 23 (1979).
16. M.-H. Whangbo, M. J. Foshee, and R. Hoffmann, *Inorg. Chem.* **19,** 1723 (1980).
17. R. Hoffmann, *J. Chem. Phys.* **39,** 1397 (1963).
18. R. Hoffmann and W. N. Lipscomb, *J. Chem. Phys.* **36,** 2179, 3489 (1962); **37,** 2872 (1962).
19. The program EHMACC produced by M.-H. Whangbo, M. Evain, T. Hughbanks, M. Kertesz, S. Wijeyesekera, C. Wilker, C. Zheng, and R. Hoffmann was used.
20. D. R. Taylor, J. C. Calabrese, and E. M. Larsen, *Inorg. Chem.* **16,** 721 (1977).
21. C. Kittel, "Introduction to Solid State Physics," 6th ed., Wiley, New York (1986).
22. J. C. Huffman, Ph.D. thesis, Indiana University (1974).
23. J. de Meulenaer and H. Tompa, *Acta Crystallogr.* **19,** 1014 (1965).
24. P. G. Lenhert, *J. Appl. Crystallogr.* **8,** 568 (1975).
25. J. H. Ammeter, H.-B. Bürgi, J. C. Thibeault, and R. Hoffmann, *J. Am. Chem. Soc.* **100,** 3686 (1978).